A Feedback Analytic Algorithm for Maximal Solar Energy Harvesting of InP Stepped Nanocylinders

Dan Wu, Zhiyang Lu, Jing Tan, Tao Lin, Yajing Liu, and Kai Wang

***Abstract*—Due to the potential for high energy harvesting capacity, subwavelength scale semiconductor nanostructured arrays are used to address the issue of single-junction thin-film solar cells' limited solar energy harvesting. Along with numerical simulations, an effective and efficient algorithm is crucial to maximizing the optical field modulation and energy trapping capacity of nanostructures. Based on the effective medium theory and the leaky mode resonance, an analytical feedback algorithm is suggested in this study to determine the precise the dimensions of vertically aligned InP stepped nanocylinders (SNCs) for maximum solar energy absorption. For both square and hexagonally arranged two-segment or three-segment InP SNC arrays, the ideal geometrical dimensions were quantitatively estimated for maximum energy harvesting. Densities of short-circuit current J_{sc}s under the AM 1.5G spectrum's illumination as the measurement standard, they were computed for each SNC array. The maximal J_{sc} of 32.85 mA/cm^2 was obtained with square three-segment InP SNC arrays. The optimized SNC arrays for the maximum light absorption are also validated and examined using thorough finite-difference time-domain computational simulations. The algorithm estimated maximum J_{sc} had tolerances of under 1.8% for all scenarios, which, when compared to simulations, shows that this analytical method offers a practical and efficient means to direct the design of high-performance InP SNC arrays solar cells.**

***Index Terms*—Algorithms, energy capture, solar energy.**

I. Introduction

THE escalating global demand for energy has resulted in the continuous advancement of clean energy sources, among which solar cells have played a significant role [1], [2]. The high percentage of energy conversion efficiency is, however, hampered by limited solar energy collection capacity. When compared to thin-film or bulk solar cells, the incorporation of semiconductor nanocylinder (NC) or nanowire arrays has emerged as an achievable solution since they can dramatically reduce material consumption while maintaining or even boosting device performance [3], [4], [5]. These advantages are mostly attributable to NCs' optical absorbing characteristics, which include improved absorption and spectrum selectivity [6], [7]. InP has a direct band gap and high electron mobility, making it one of the most widely utilized III-V semiconductor materials for solar cells [8]. Wanlass M. et al. reported that the maximum conversion efficiency of InP crystalline cell reached $24.2 \pm 0.5\%$ [9].

In addition to material characteristics, semiconductor NC arrays' three-dimensional geometrical factors and arrangement play a key role in controlling their optical qualities [10], [11], [12], [13], [14]. Therefore, improving the morphology and topology of semiconductor NCs is essential to increase their solar spectrum capture efficiency. The three-dimensional geometric parameters of the NC arrays usually include diameter (D), periodicity (P), length (L), and the way of arrangement. Reports have shown that adjusting the diameter of the NC can significantly modulate the absorption feature of the incident spectrum due to the corresponding various resonance modes [10], [15], [16], [17]. It is also claimed that simultaneous activation of the HE_{11} and HE_{12} resonant modes will boost the NCs' ability to absorb light. Additionally, it is discovered that the InP NC arrays will exhibit higher light absorption efficiency with the proper filling ratio, which is defined as the percentage of the volume of the semiconductor material compared with the total volume of the periodic cell [10], [11], [16], [19], [20]. This is explained by the reason that a less proportion of light is reflected and transmitted [21], [22], which enhances scattering and lengthens the optical path to raise the probability of photon absorption [20]. Additionally, some researches have emphasized the significance of modifying NC length [23], [24], [25], [26]. In general, increasing the length of the NC arrays can improve the absorption, but this improvement in the wide area of surface to volume ratio may also increase the loss of nonradiative recombination due to faults at the side surface, let alone the difficulties of fabricating the NCs. Therefore, choosing the appropriate length to balance between increasing light absorption and limiting surface recombination is also essential in obtaining the maximum solar energy harvesting [27].

Manuscript received 13 October 2023; revised 26 December 2023; accepted 8 January 2024. Date of publication 15 January 2024; date of current version 29 January 2024. This work was supported in part by the Natural Science Foundation of Top Talent of Shenzhen Technology University (SZTU) under Grants GDRC202110 and 2019210, in part by the Guangdong Basic and Applied Basic Research Foundation under Grant 2022A1515011071, in part by Shenzhen Stable Support Research Foundation under Grant 20220717215521001, in part by the Communication University of Zhejiang Talent Research and Creation Found under Grant Z301B21510, in part by the Instruments Development Projects of Shenzhen Technology University under Grant JSZZ202201019, and in part by the Education Department of Guangdong Province under Grant 2021KCXTD045. *(Dan Wu and Zhiyang Lu contributed equally to this work.) (Corresponding author: Yajing Liu.)*

Dan Wu, Zhiyang Lu, Jing Tan, and Tao Lin are with the College of New Materials and New Energies, Shenzhen Technology University, Shenzhen 518118, China (e-mail: wudan@sztu.edu.cn; 2100413003@stumail.sztu.edu.cn; 2210412030@stumail.sztu.edu.cn; lintao@sztu.edu.cn).

Yajing Liu is with the School of Art and Design, Communication University of Zhejiang, Hangzhou 310018, China (e-mail: irenelove1104@163.com).

Kai Wang is with the Institute of Nanoscience and Applications, Department of Electronic and Electrical Engineering, Southern University of Science and Technology, Shenzhen 518055, China (e-mail: wangk@sustech.edu.cn).

This article has supplementary downloadable material available at https://doi.org/10.1109/JPHOT.2024.3353787, provided by the authors.

Digital Object Identifier 10.1109/JPHOT.2024.3353787

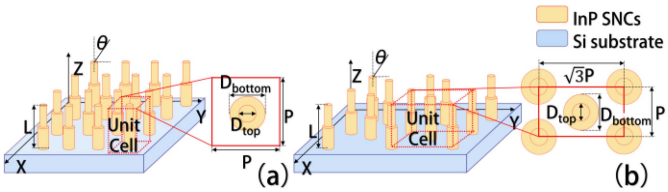

Fig. 1. Schematics of two-segment InP SNC arrays that are vertically aligned, where (a) and (b) represent square and hexagonal SNC arrays, respectively, with insets describing the parameters in each unit cell.

The optimization target to obtain near unity light absorption of the incident spectrum within the critical wavelength of the active layer material is the ideal case for energy harvesting. Multiple different parameters should be optimized at the same time in light of the NCs' geometrical dimensions and layout. The majority of the reported geometrical dimensions for NC arrays with the high light-capture efficiency, are usually local optimal solutions in the given parameter space. The multi-parameter optimization problem is typically solved using time-consuming numerical simulations [10], [11]. Our group has previously reported an analytical technique for finding the geometric parameters of vertically aligned single, double, and multiple diameter nanowire arrays with high aspect ratio that may be used with different semiconductor materials [18]. Compared with the high aspect ratio of nanowire arrays, stepped nanocylinder (SNC) arrays are much more easily to be fabricated such as the polystyrene nanosphere assisted etching method [28]. Despite the SNCs' best features, there are few studies of this type of structure for maximal light harvesting, which restricts their use in solar cell light gathering.

In this paper, to maximize solar energy collecting, a feedback analytical approach for optimizing SNCs' geometrical design is proposed. In the algorithm, the range of the diameters of SNC are sorted by joint consideration of leaky mode resonance and Mie theory whereas an effective medium layer is also constructed by obtaining the specific values of the periodicity and diameters of each segment of the SNC structure to maximize light absorption. The algorithm is used to thoroughly evaluate two-segment and three-segment SNC arrays in order to determine the ideal geometric parameters that apply to square and hexagonal arrangements. In the meantime, thorough numerical simulations are run to further validate the proposed algorithm. It is demonstrated that this method is useful in directing the design of SNC arrays photovoltaic cells by the calculated maximal photocurrent density of the SNC arrays, which has a low tolerance with the findings of numerical simulation but with a greater calculation efficiency.

II. Development of the Feedback Analytical Algorithm of InP SNC Arrays for Maximal Solar Energy Harvesting

A. Model of the InP SNC Arrays

As schematically depicted in Fig. 1, two-segment InP SNC arrays are vertically aligned and are standing on a Si substrate in either a square or hexagonal layout for the purpose of algorithm development. The insets of Fig. 1(a) and (b) in periodic unit cells describe the corresponding dimensions for each arrangement. The majority of InP NC-based solar cell topologies agree with this configuration of the SNC arrays [29], [30]. Each unit cell contains NCs with different diameters labeled as D_{bottom} and D_{top}. The spacing between the centers of neighboring SNCs, which has the same value for squarely aligned SNCs but is different for hexagonally aligned SNC arrays, determines the periodicity (P). Each SNC's entire length is denoted by the variable L, which is set to 2 μm since It is long enough to successfully adsorb more than 90% of the incident radiation [31], and each segment's height is equal to L/2. The concept of FR_{global} is defined as the volume ratio of the InP material to the volume in each unit cell. Thus, the FR_{global} of the square arranged SNC arrays can be expressed as $\sum_{i=1}^{i=m} \pi * D_i^2/(4 * m * P^2)$, where m represents the number of segments of the SNCs. The FR_{global} has the maximal value of $\pi/4$, and in this scenario, the SNCs occupy the highest proportion of the unit cell, resulting in the transformation of the SNC structure into NC structure [32]. In the same vein, the FR_{global} for hexagonal SNC arrays is denoted as $\sum_{i=1}^{i=m} \pi * D_i^2/(4 * 3^{1/2} * m * P^2)$ with the maximal value of $\pi * 3^{1/2}/6$.

B. Algorithm Development of the SNC Arrays for Maximal Solar Energy Harvesting

Fig. 2 illustrates the flowchart of the proposed feedback analytical algorithm. Specifically, the excitation of the leaky mode resonances of HE_{11} and HE_{12} and the adoption of the Mie theory will provide the range of the optimal diameters. Secondly, for a given SNC array, there is a global filling ratio FR_{global} and segment filling ratios FR_{seg}s for each segment layer of the SNC array. For each segment layer, an effective medium layer will be created. These equivalent layers will then be applied of Fresnel's law to calculate light absorption of the SNC arrays. Maximal light harvesting is set as the design target and in this case the short-circuit current density J_{sc} is chosen as the evaluation parameter. By receiving feedback and undergoing circulation within the specified parameter spaces, the optimal geometrical dimensions of the SNC arrays will be determined, leading to the achievement of maximum light harvesting. The refractive index for both the InP and the Si are obtained from Palik's material database. The incident spectrum restricts the high energy region to the blue end, specifically at 300 nm. On the other hand, the absorbing region is limited at the red end by the critical wavelength of 925 nm, which corresponds to the bandgap of InP at 1.34 eV. After obtained the light absorption spectrum, the light harvesting of the AM 1.5G spectrum is evaluated by the short-circuit photocurrent density of SNCs as (1), where the q is elementary charge, the h is Planck constant, the c is velocity of light, the $A(\lambda)$ is the absorption spectrum of each SNC arrays, and the $N(\lambda)$ is the number of photons every unit area every second for the wavelength of the incident light from the standard solar spectrum. The upper and lower limits of the formula are given by the cut-off frequency of InP material and the spectral range of AM 1.5G. The formula for calculating the

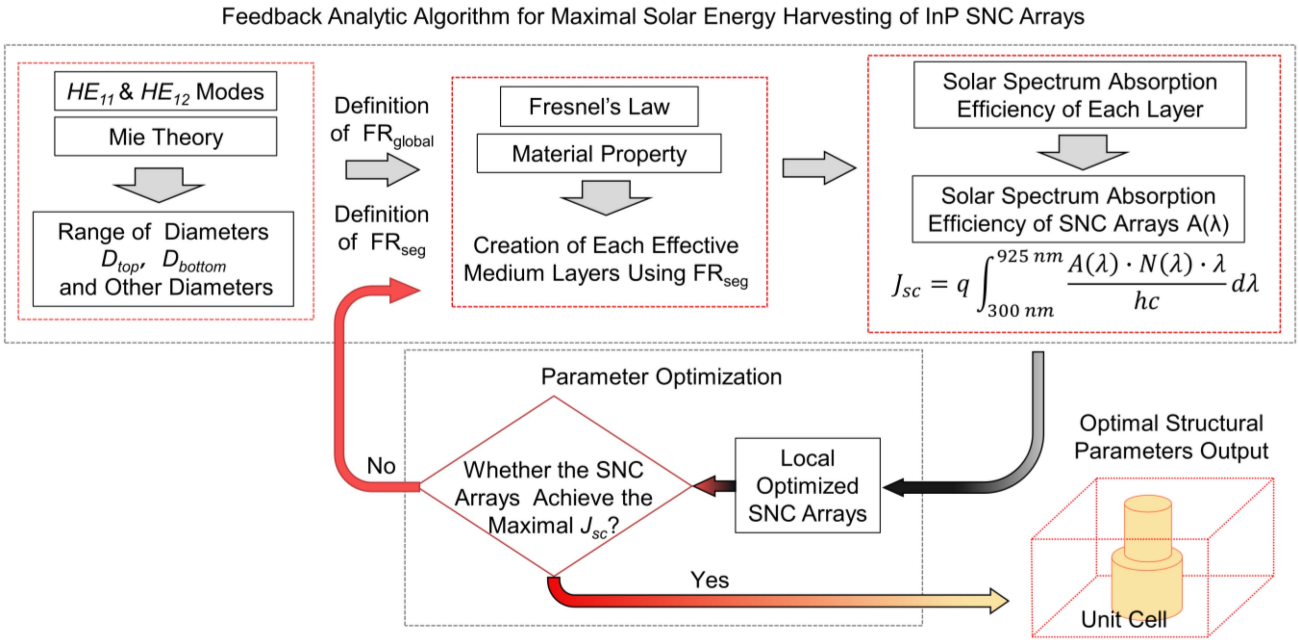

Fig. 2. Flow chart of feedback algorithm of InP SNC arrays for maximal solar energy harvesting.

photocurrent density is

$$J_{sc} = q \int_{300\,nm}^{925\,nm} \frac{A(\lambda) \cdot N(\lambda) \cdot \lambda}{hc} d\lambda. \tag{1}$$

1) Range of Respective Diameters of SNC Arrays: The objective is to achieve the maximal solar energy harvesting through optimal structural and arrangement of InP SNC arrays. To increase the light absorption, previous research has proven that InP nanowires supporting two resonant modes located within the absorbing region has the greatest potential in improving light absorption [31]. Furthermore, accompanying with Mie theory and leaky mode resonance, an optimal diameter value for maximal light harvesting can be determined [18]. However, the previous method cannot be directly applied to the InP SNC arrays. This is because for each SNC, there are more than one segment with different diameters and the length of each segment is only half or one third of the length of the previous work. This reduction of length will lead to great deviation from the results predicted by the previous method which assumed the large aspect ratio of the nanowires indicating of at least ten times of length to diameter. Therefore, the adoption of the Mie theory and leaky mode resonance can only provide the range of the diameters of the SNCs and the specific optimal value will be found through feedback optimization.

Based on the illustration in Fig. 2, the absorption of vertically-aligned SNCs is mainly attributed to the effective excitation of HE_{1m} modes. This is due to the antisymmetric in-plane field distribution of the incident plane waves. Within the region of the spectrum constrained by the solar spectrum and the critical wavelength of the InP, there should be two fundamental modes. In addition, these HE_{1m} modes fulfill the eigenvalue equations, and the resonant wavelengths can be determined when the real part of the propagation constant of the mode along the SNC axial direction tends to zero, as depicted in

$$\frac{\varepsilon_1}{k_1} \frac{J'_1(k_1 R_{seg})}{J_1(k_1 R_{seg})} - \frac{\varepsilon_2}{k_2} \frac{H_1^{(1)'}(k_2 R_{seg})}{H_1^{(1)}(k_2 R_{seg})} = 0, \tag{2}$$

where, k_1 and k_2 are transverse components of the wave vector inside and in the air surrounding of the SNC, ε_1 and ε_2 are their respective dielectric constants, J_1 and $H_1^{(1)}$ are the first-order Bessel function and Hankel function of the first kind respectively, and R_{seg} is the radius of the segment of the SNC. Therefore, the diameters can be calculated by (3) to (5) and for InP materials the diameters fall in the range of 120 to 200 nm. After obtaining the range of the diameters, increment is chosen as 5 nm and then the respective diameters will be included into the algorithm for circulation until the optimal values are obtained. The absorption of SNCs with unpolarized incidence light calculated by Mie theory [33] is shown as below.where k_0 is the modulus of the incident light propagation constant, footnote *i* refers to the corresponding function of the *i*th order, and *n* refers to the complex refractive index.

$$Q_{abs} = \frac{1}{k_0 R_{seg}} \left[Re\left(\sum_{i=-\infty}^{\infty} b_i \right) + Re\left(\sum_{i=-\infty}^{\infty} a_i \right) \right] - \frac{2}{k_0 R_{seg}} \sum_{i=-\infty}^{\infty} \left(|b_i|^2 + |a_i|^2 \right), \tag{3}$$

$$a_i = \frac{n J_i(nk_0 R_{seg}) J'_i(k_0 R_{seg}) - J_i(k_0 R_{seg}) J'_i(nk_0 R_{seg})}{n H'_i(k_0 R_{seg}) J_i(nk_0 R_{seg}) - J'_i(nk_0 R_{seg}) H_i(k_0 R_{seg})}, \tag{4}$$

$$b_i = \frac{J_i(nk_0 R_{seg}) J'_i(k_0 R_{seg}) - n J_i(k_0 R_{seg}) J'_i(nk_0 R_{seg})}{J_i(nk_0 R_{seg}) H'_i(k_0 R_{seg}) - n J'_i(nk_0 R_{seg}) H_i(k_0 R_{seg})}. \tag{5}$$

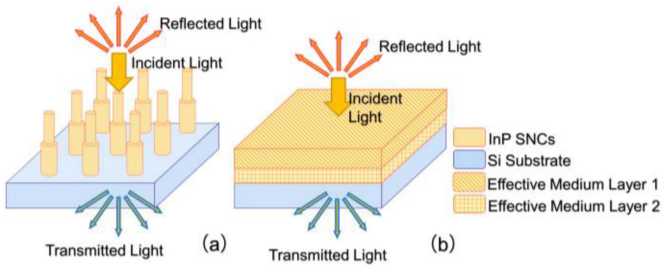

Fig. 3. Light reflection, transmission and absorption of (a) SNCs and (b) effective medium layers for each segment layer.

2) Calculation of $\mathrm{FR_{seg}s}$*, Periodicities, and Diameters of SNC Arrays:* An effective medium layer is created as shown in Fig. 3 with a complex refractive index to accurately portray the refraction and transmission characteristics of the SNC arrays. Thus, the geometrical dimension parameters of the InP SNCs such as the periodicities and diameters of each segment of the SNCs are temporarily excluded from the calculation. Therefore, by utilizing Fresnel's law, it is possible to compute the reflection and transmission of the effective medium layer. This calculation can indirectly reveal the characteristics of the SNC arrays. However, the diffraction property, along with other aspects of the light-matter interaction within this medium layer, is not taken into account. It is noted that SNC arrays should be considered as a multi-layer film with the number of layers being consistent with the number of segments, rather than a single-layer equivalent film. According to the definition of the two segments InP SNC arrays, the FR_{global} can be calculated as

$$\begin{aligned} FR_{global} &= \frac{\pi D_{top}^2/4 \times \frac{L}{2} + \pi D_{bottom}^2/4 \times \frac{L}{2}}{P^2 \times L} \\ &= \frac{\pi D_{top}^2/4 \times \frac{L}{2}}{P^2 \times L} + \frac{\pi D_{top}^2/4 \times \frac{L}{2}}{P^2 \times L} \\ &= \frac{FR_{seg-top} + FR_{seg-bottom}}{2}. \end{aligned} \tag{6}$$

Therefore, once given the range of the FR_{global} and the diameters range of the top segment and the bottom segment are sorted according to the previous section, the periodicity as well as the $FR_{seg\text{-}top}$ and $FR_{seg\text{-}bottom}$ can be determined in sequence. Then the creation of the effective medium layer of the top segment and the bottom segment can be realized. The light absorption of the InP SNC arrays can be separately calculated and the solar spectrum absorption is obtained as the sum of the top and bottom effective medium layer.

The Bruggeman formula is adopted to calculate the refractive index of the effective medium layer as

$$(1 - FR_{seg}) \frac{\varepsilon_{\text{air}}^2 - \varepsilon_{\text{em}}^2}{\varepsilon_{\text{air}}^2 + 2\varepsilon_{\text{em}}^2} + FR_{seg} \frac{\varepsilon_{\text{SNC}}^2 - \varepsilon_{\text{em}}^2}{\varepsilon_{\text{SNC}}^2 + 2\varepsilon_{\text{em}}^2} = 0, \tag{7}$$

wherein, ε_{air}, ε_{SNC} and ε_{em} represent the dielectric constant of vacuum, SNCs and effective medium layer respectively [31]. The FR_{seg} represent the material portion of each segment layer within the unit cell rather than the FR_{global}. The imaginary and real parts of the refractive index of the effective medium layer are described as:

$$n_{\text{em-real}} = Re\left(\sqrt{\varepsilon_{\text{em}}}\right), \tag{8}$$

$$n_{\text{em-imag}} = \sqrt{\frac{-A + \sqrt{A^2 + B^2}}{2}}, \tag{9}$$

$$\begin{aligned} \mathrm{A} = {} & FR_{seg}\left(n_{\text{SNC-real}}^2 - n_{\text{SNC-imag}}^2\right) \\ & + (1 - FR_{seg})\left(n_{\text{air-real}}^2 - n_{\text{air-imag}}^2\right), \end{aligned} \tag{10}$$

$$\begin{aligned} B = {} & 2FR_{seg} n_{\text{SNC-real}}\, n_{\text{SNC-imag}} \\ & + 2\left(1 - FR_{seg}\right) n_{\text{air-real}}\, n_{\text{air-imag}}, \end{aligned} \tag{11}$$

where $n_{SNC\text{-}real}$ and $n_{SNC\text{-}imag}$ represent the real and imaginary parts of the refractive index of SNC materials [31]. $n_{air\text{-}real}$ and $n_{air\text{-}imag}$ represent the real and imaginary parts of the vacuum refractive index. After the construction of this efficient medium layer, the reflection and transmission can be calculated using Fresnel's law. Additionally, the film's light absorption can be determined by

$$A(\lambda) = 1 - T(\lambda) - R(\lambda), \tag{12}$$

where the $A(\lambda)$ is the SNC array's absorption as a function of the incoming wavelength. From the equation above, it is clear that maximal light absorption current can be achieved by minimizing reflection and transmission [22].

In this work, to further verify the suggested algorithm, Ansys FDTD (Lumerical FDTD Solutions 8.24) is also used. Numerical models are built for the optimal InP SNC arrays and optical field analysis is carried out. The incident spectrum of the planewave light source is set from 300 to 925 nm.

III. Results and Discussion

Two-segment and three-segment InP SNC arrays of square and hexagonal arrangements are optimized for maximal light energy harvesting. In the meantime, numerical simulations using FDTD are presented below in order to validate the proposed method and conduct tolerance analysis.

A. Maximal Light Harvesting for Square and Hexagonal Three-Segment SNC Arrays

In Fig. 4, it is illustrated that the absorption efficiency of the effective medium layer in both the square and hexagonal two-segment InP SNC arrays. Since the arrangement of the SNC arrays affect little on the creation of the effective medium layer, for each FR_{global} and the given range of the D_{top} and D_{bottom}, the periodicity for a certain SNC array can be obtained, following by the calculation of the $FR_{seg\text{-}top}$ and $FR_{seg\text{-}bottom}$. Therefore, the effective medium layer for the top segment layer and the bottom segment layer are created. Through calculation of the absorption efficiency of the top and the bottom effective medium layer and the sum of the two parts, the total absorption of the InP SNC array can be obtained. The light absorption efficiency initially rises, reaches a maximal, and then gradually decreases as the FR_{global} increases. Respective $FR_{seg\text{-}top}$, $FR_{seg\text{-}bottom}$ as the change of

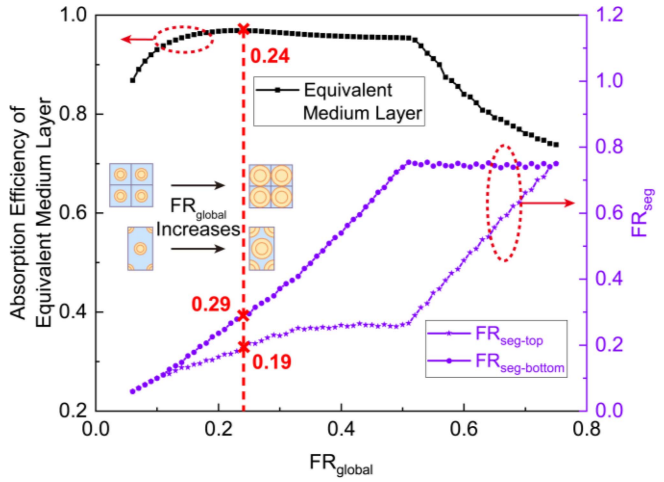

Fig. 4. Absorption efficiency of the effective medium layer in two-segment InP SNC arrays can be expressed as a function of FR_{global} and the change in FR_{seg} with varying FR_{global}.

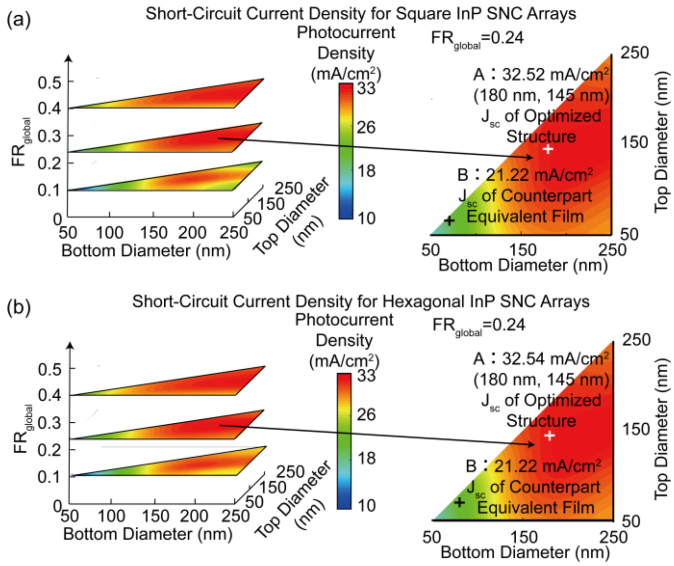

Fig. 5. Short-circuit current densities in relation to top, bottom, and FR_{global} diameters. Two-segment InP SNC arrays that are (a) square and (b) hexagonal; the insets illustrate the ideal geometrical dimensions for the corresponding SNC arrangements.

the FR_{global} are also shown in Fig. 4. This is due to changes in the transmitted and reflected light caused by changes in the complex refractive indices of the effective medium layer resulting from the FR_{global} variation. With an increase in FR_{global} from 0.05 to 0.24, the inclusion of InP material results in a greater absorption of light within the effective medium layer before the transmission. The aforementioned pattern continues until the FR_{global} reaches a value of 0.24. Beyond this point, the increasing of refractive indices within the equivalent layer creates optical impedance between the air and SNC arrays. Consequently, the reflectance at the incident surface increases, leading to a reduction in light absorption. If the FR_{global} is too large, the reflection at the air/InP SNC arrays interface will be increased leading to the decrease of the absorption. It is also worth noticing that the creation of the effective medium layer will overlook the way of arrangement. Consequently, the square and hexagonal arrays will have the same optimal FR_{global} of 0.24. However, they will have different periodicities, with the square arrangement having a periodicity of 295.66 nm and the hexagonal arrangement having a periodicity of 317.71 nm.

Fig. 5 presents a summary of the changes in short-circuit current densities with respect to D_{top} and D_{bottom}, as well as FR_{global}, for two different types of SNC arrays. In general, light harvesting increases with FR_{global}, reaches its maximum value, and then decreases. The insets in Fig. 5 show the greatest J_{sc} of 32.52 and 32.54 mA/cm^2 for both square and hexagonal InP SNCs at FR_{global} of 0.24. The tolerances for square and hexagonal SNCs are within 1.75% of the of the simulation-derived maximum values of 33.10 and 33.12 mA/cm^2. In the insets of Fig. 5(a) and (b), the maximum J_{sc} for the ideal geometric parameters determined by the feedback method is indicated by point A. Point B is the maximal short-circuit current density result of film with equal volume InP material. Compared with planar film sample of the same amount InP material with the photocurrent of 21.22 mA/cm^2 which marked as black cross, the SNC structure has a 53.25% higher absorption efficiency.

The structure parameters obtained by the algorithm require D_{top} to be 145 nm and D_{bottom} to be 180 nm for both square and hexagonal InP SNC arrays. When the D_{top}, D_{bottom}, and FR_{global} is the same for both arrangements, according to the schematic of the unit cell, the $(P_{square}/P_{hexagonal})^2$ is $\sqrt{3}/2$. With less mode coupling among SNCs than square arrays, the $P_{hexagonal}$ is 1.07 times larger than the P_{square}. When the FR_{global} is 0.1, the J_{sc} values of the SNC arrays with square and hexagonal arrangements are 31.85 and 32.08 mA/cm^2, respectively. Similarly, when the FR_{global} is 0.4, the J_{sc} values of the SNC arrays with square and hexagonal arrangements are 32.87 and 32.88 mA/cm^2, respectively. It is evident that the difference in maximum J_{sc} values for each FR_{global} is not significant. This can be attributed to the high absorption efficiency of individual SNCs rather than the mode coupling.

The above analysis indicates little influence of the arrangement of the InP SNCs and to further analyze the nature of the light harvesting, the electric field distributions at the cross-sectional view of the square SNC arrays in the unit cell are analyzed as shown in Fig. 6. Based on the leaky mode resonance, the resonant wavelengths of diameters of 145 nm and 180 nm are calculated to be at 429 nm, 447 nm, 678 nm and 825 nm respectively. Therefore, using these wavelengths as the incident wavelength respectively, the electric field cross-sectional diagram can be obtained in Fig. 6. As observed in Fig. 6(a) and (b), the electric field intensity near the interface between air and InP SNC arrays is lower in the SNC structures than in the planar counterpart, which is attributed to the less reflection at the interface. As can be seen from Fig. 6(a)–(d), the material itself has better absorption of short wave, which makes almost no energy transmitted out, so the main consideration here is to reduce the loss caused by reflection. From Fig. 6, it is obvious to find that the optimized structure has a better anti-reflection effect

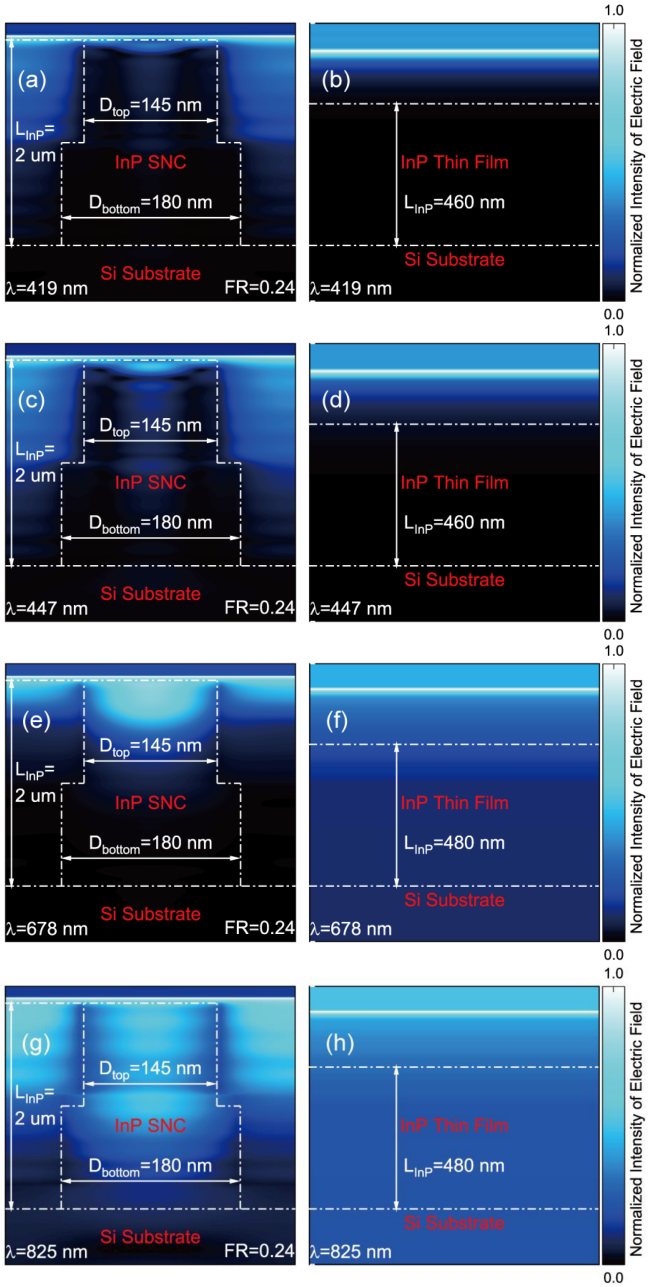

Fig. 6. Normalized electric field intensity of two-segment InP SNC arrays and equal-volume InP thin film structure. (a), (c), (e) And (g) square two-segment InP SNC unit (optimized structure); (b), (d), (f) and (h) are the equal-volume InP thin film structure.

than the thin film structure, which allows more incident light to enter the SNC array and then be absorbed. When the incident wavelength is 678 nm, the light energy is mainly absorbed by the top segment of the InP SNC as shown in Fig. 6(e). When the incident wavelength is 825 nm, the light energy is absorbed by both the top and the bottom segment due to the change of the imaginary part of the refractive index. For the planar sample with equal volume of InP material, the light penetration depth is short when the incident wavelength is 678 nm as shown in Fig. 6(f) but with higher light absorption efficiency as shown

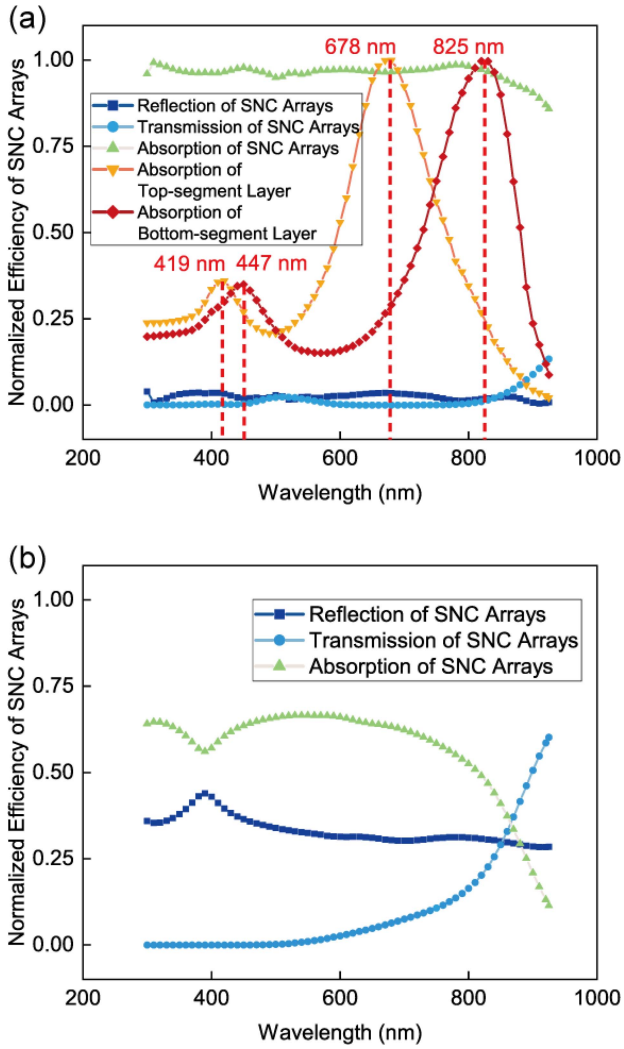

Fig. 7. Light absorption, reflection and transmission of (a) two-segment InP SNC arrays and (b) equal-volume InP thin film structure.

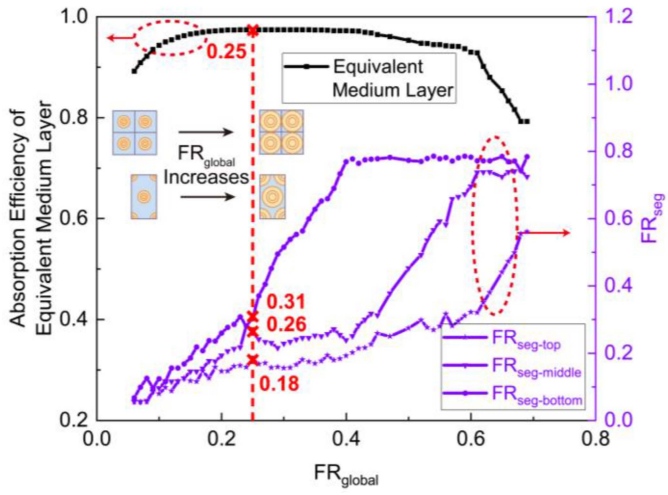

Fig. 8. Absorption efficiency of the effective medium layer in three-segment InP SNC arrays can be expressed as a function of FR_{global} and the change in FR_{seg} with varying FR_{global}.

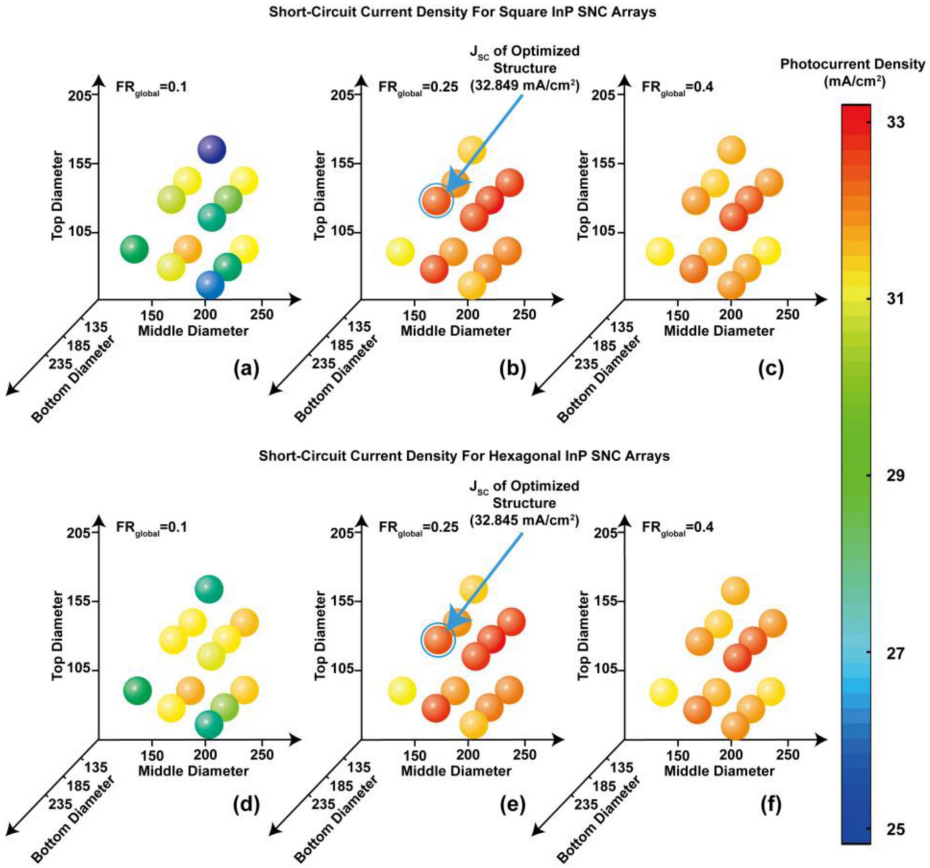

Fig. 9. Short-circuit current densities as a function of D_{top}, D_{middle}, D_{bottom} and FR_{global}. (a), (b), (c) Corresponds to the square whereas (d), (e), (f) corresponds to the hexagonal three-segment arrays. (a) And (d) with FR_{global} of 0.1, (b) and (e) with FR_{global} of 0.25, and (c) and (f) with FR_{global} of 0.4 respectively. The blue circle marks on each indicating the maximal J_{sc} for respective SNC arrangements.

in Fig. 6(g). The light absorbing efficiency is much lower at the 825 nm which is due to the low absorbing coefficient at the longer wavelength. In addition, the resonant wave electric field distributions of the hexagonal arrays are shown in Fig. S1 in the supporting information.

Meanwhile, light absorption, reflection, and transmission efficiency of square two-segment InP SNC arrays optimized by the algorithm and that of an equal-volume InP thin film is shown in Fig. 7. In Fig. 7(a), the optimized SNC structures exhibit more than 90% absorption efficiency across the incident spectrum. Additionally, the normalized absorption curves calculated by the Mie theory for diameters of 145 nm and 180 nm are also displayed in Fig. 7(a). Two resonant modes are excited for the top and bottom segment of the SNC arrays with peak wavelength of 678 nm and 825 nm. In contrast, the equal-volume thin film structure in Fig. 7(b) shows more reflection and transmission of electric field intensity, leading to lower absorption. On the other hand, the poor absorption performance of the thin film structure is mainly due to reflection of about 30% of the light in solar spectrum. Moreover, as the wavelength increases, more light is transmitted out, leading to lower absorption efficiency, which can even be as low as 10%. In Fig. S4(a), the absorption curve of the hexagonal arrays is almost not much different from that of the square arrays, which also reflects that the photocurrent density of the optimized structure is almost no longer affected by the arrangement.

B. Maximal Light Harvesting for Square and Hexagonal Three-Segment SNC Arrays

The algorithm can also be applied for the optimization of the geometric parameters of the three-segment InP SNC arrays for maximal solar energy harvesting. For each FR_{segs}, the value of the D_{top}, D_{middle}, and D_{bottom}, and the periodicity can be calculated after rounds of feedback circulation. Correspondingly, FR_{seg_top}, FR_{seg_middle}, and FR_{seg_bottom} are obtained and therefore the effective medium layer of each segment is constructed. The light absorption of the three- segment InP SNC arrays is obtained as the sum of the light absorption of the three effective medium layers calculated by the Fresnel's law. After the feedback circulation across the four parameter spaces of the FR_{global}, D_{top}, D_{middle}, and D_{bottom}, the optimal FR_{global} value of 0.25 is found which is applicable to both the square and hexagonal arrays as exhibited by the results in Fig. 8. The individual FR_{top}, FR_{middle}, and FR_{global} are 0.18, 0.26, and 0.31 respectively. Following the calculations above, the periodicities for square and hexagonal SNC arrays are determined to be 346.42 nm and 372.26 nm, respectively.

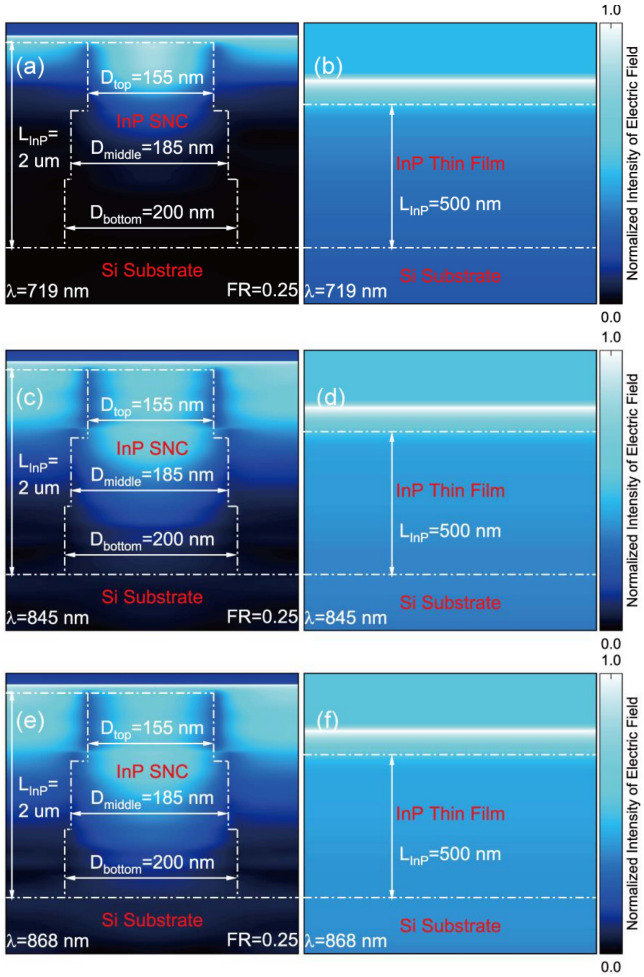

Fig. 10. Electric field normalized intensity of three-segment InP SNC arrays. (a), (c) And (e) square three-segment InP SNC (optimized structure); (b), (d) and (f) equal-volume InP thin film structure.

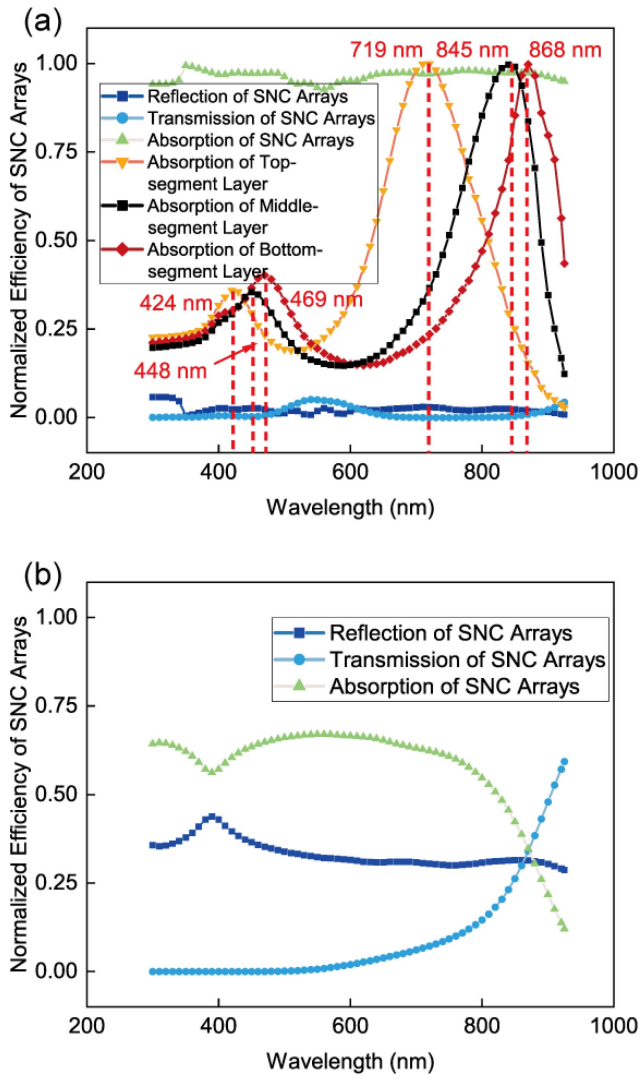

Fig. 11. Light absorption, reflection and transmission of (a) three-segment InP SNC arrays and (b) equal-volume InP thin film structure.

The structure parameters optimized by the algorithm require D_{top} to be 155 nm, D_{middle} to be 185 nm and D_{bottom} to be 200 nm. Fig. 9 provides a summary of the J_{sc} variation as a function of D_{top}, D_{middle}, D_{bottom} and FR_{global} for two types of SNC arrays both by the proposed algorithm and the numerical simulations. In general, light harvesting increases with FR_{global}, reaches its maximum value, and then decreases. Fig. 9 shows that the highest J_{sc} of square and hexagonal InP SNC are 33.20 and 33.19 mA/cm^2 based on the numerical simulations, and the corresponding J_{sc} of the optimized structure are 32.85 and 32.85 mA/cm^2 from the proposed algorithm with the tolerance of 1.05%.

Figs. 10 and 11 compare and analyze the electric field distributions and light absorption, reflection, and transmission efficiencies between the equal volume InP thin film structure and the optimized square three-segment InP SNC structure. In Fig. 10(a)–(f), it can be seen that the optimized structures have lower reflection and transmission electric field intensity compared to the film structure, indicating higher light trapping efficiency, which can also be further verified by Fig. 11. In addition, other resonant wave electric field distributions of the square arrays are shown in Fig. S2 of the supporting information, and all resonant wave electric field distributions of the hexagonal arrays are shown in Fig. S2 of the supporting information.

Additionally, the normalized absorption curves calculated by the Mie theory for which the absorption peaks locating at 719 nm, 845 nm, and 868 nm are also displayed corresponding to the absorption peak wavelengths obtained through the excitation of leaky resonant modes at the diameter of 155 nm, 185 nm and 200 nm, respectively. On the other hand, the current equal volume film has a thickness of 0.5 um and its absorption curve remains largely unchanged when compared to the previous film with a thickness of 0.46 um. The absorption curve of the optimized square three-segment InP SNC structure shows that it can achieve an absorption efficiency of almost 100% within the absorption range, surpassing the equal volume film structure. This implies that the three-segment structure has better absorption in the long-wave portion when compared to the optimized two-segment structure. In Fig. S4(b), the absorption curve of the hexagonal arrays is almost not much different from that of the square arrays.

IV. Conclusion

In this study, for both squarely and hexagonally aligned InP SNC arrays, a feedback analytical technique is described to produce the best light harvesting for the highest solar energy harvesting. Quantitative calculations were performed to determine the ideal geometrical dimensions for both square and hexagonally arranged two-segment or three-segment InP SNC arrays. When compared to time-consuming FDTD simulations, the predicted maximum J_{sc} with derived multivariate SNC arrays remains below 1.75% for all circumstances. The corresponding diameter range is obtained by Mie theory and leaky mode resonance. Additionally, regardless of how the SNCs are arranged, the FR_{global} of two-segment and three-segment SNC arrays is tuned to be 0.24 and 0.25, respectively. The FR_{global}, $FR_{seg}s$, periodicities and specific diameters of each segment are calculated by effective medium layers. When the geometrical parameters are optimal, the configurations of SNC arrays have little impact on light absorption, but at high FR_{global} values, coupling between neighboring SNCs becomes crucial for SNCs. The greatest short-circuit current densities estimated for the two-segment SNC arrays in square and hexagonal arrangements were 32.52 and 32.54 mA/cm^2, respectively. Furthermore, highest short-circuit current densities of 32.85 and 32.85 mA/cm^2 were obtained for two-segment SNC arrays arranged in square and hexagonal arrangement, respectively. Due to no preference of the materials selection, the proposed algorithm can be further applied to other commonly photovoltaic materials. The proposed design demonstrates high precision with wide suitability and time-efficiency for practical SNC-based solar cell design, making it a promising tool in the field of maximizing light capture.

References

[1] H. Yao and J. Hou, "Recent advances in single-junction organic solar cells," *Angewandte Chemie*, vol. 61, no. 37, Sep. 2022, Art. no. e202209021.

[2] R. Wang, T. Huang, J. Xue, J. Tong, K. Zhu, and Y. Yang, "Prospects for metal halide perovskite-based tandem solar cells," *Nature Photon.*, vol. 15, no. 6, pp. 411–425, Jun. 2021.

[3] P. Spinelli, M. A. Verschuuren, and A. Polman, "Broadband omnidirectional antireflection coating based on subwavelength surface Mie resonators," *Nature Commun.*, vol. 3, no. 1, Feb. 2012, Art. no. 692.

[4] L. Cao, J. S. White, J.-S. Park, J. A. Schuller, B. M. Clemens, and M. L. Brongersma, "Engineering light absorption in semiconductor nanowire devices," *Nature Mater.*, vol. 8, no. 8, pp. 643–647, Aug. 2009.

[5] B. M. Kayes et al., "27.6% conversion efficiency, a new record for single-junction solar cells under 1 sun illumination," in *Proc. IEEE 37th Photovolt. Specialists Conf.*, 2011, pp. 000004–000008.

[6] M. L. Brongersma, Y. Cui, and S. Fan, "Light management for photovoltaics using high-index nanostructures," *Nature Mater.*, vol. 13, no. 5, pp. 451–460, May 2014.

[7] L. Cao, P. Fan, E. S. Barnard, A. M. Brown, and M. L. Brongersma, "Tuning the color of silicon nanostructures," *Nano Lett.*, vol. 10, no. 7, pp. 2649–2654, Jul. 2010.

[8] O. L. Muskens, J. G. Rivas, R. E. Algra, E. Bakkers, and A. Lagendijk, "Design of light scattering in nanowire materials for photovoltaic applications," *Nano Lett.*, vol. 8, no. 9, pp. 2638–2642, Sep. 2008.

[9] M. A. Green et al., "Solar cell efficiency tables (version 61)," *Prog. Photovolt.: Res. Appl.*, vol. 31, no. 1, pp. 3–16, Jan. 2023.

[10] P. Kailuweit, M. Peters, J. Leene, K. Mergenthaler, F. Dimroth, and A. W. Bett, "Numerical simulations of absorption properties of InP nanowires for solar cell applications," *Prog. Photovolt.*, vol. 20, no. 8, pp. 945–953, Dec. 2012.

[11] J. Kupec and B. Witzigmann, "Computational electromagnetics for nanowire solar cells," *J. Comput. Electron.*, vol. 11, no. 2, pp. 153–165, Jun. 2012.

[12] X. Zhang, X. H. Sun, and L. D. Jiang, "Absorption enhancement using nanoneedle array for solar cell," *Appl. Phys. Lett.*, vol. 103, no. 21, Nov. 2013, Art. no. 211110.

[13] A. Dorodnyy, E. Alarcon-Llado, V. Shklover, C. Hafner, A. F. I. Morral, and J. Leuthold, "Efficient multiterminal spectrum splitting via a nanowire array solar cell," *Amer. Chem. Soc. Photon.*, vol. 2, no. 9, pp. 1284–1288, Sep. 2015.

[14] S. L. Diedenhofen, O. T. A. Janssen, G. Grzela, E. Bakkers, and J. G. Rivas, "Strong geometrical dependence of the absorption of light in arrays of semiconductor nanowires," *Amer. Chem. Soc. Nano*, vol. 5, no. 3, pp. 2316–2323, Mar. 2011.

[15] W. T. Dai, D. Yap, and G. Chen, "Wideband enhancement of infrared absorption in a direct band-gap semiconductor by using non-absorptive pyramids," *Opt. Exp.*, vol. 20, no. 14, pp. A519–A529, Jul. 2012.

[16] R. Y. Zhang, B. Shao, J. R. Dong, J. C. Zhang, and H. Yang, "Absorption enhancement analysis of crystalline Si thin film solar cells based on broadband antireflection nanocone grating," *J. Appl. Phys.*, vol. 110, no. 11, Dec. 2011, Art. no. 113105.

[17] S. L. Wu, C. Zhang, X. F. Li, and Y. H. Zhan, "Proximity effect assisted absorption enhancement in thin film with locally clustered nanoholes," *Opt. Lett.*, vol. 40, no. 5, pp. 792–795, Mar. 2015.

[18] D. Wu, X. Tang, K. Wang, Z. He, and X. Li, "An efficient and effective design of InP nanowires for maximal solar energy harvesting," *Nanoscale Res. Lett.*, vol. 12, no. 1, Nov. 2017, Art. no. 604.

[19] N. M. Ali and N. H. Rafat, "Modeling and simulation of nanorods photovoltaic solar cells: A review," *Renewable Sustain. Energy Rev.*, vol. 68, pp. 212–220, Feb. 2017.

[20] P. Yu, J. Wu, S. T. Liu, J. Xiong, C. Jagadish, and Z. M. M. Wang, "Design and fabrication of silicon nanowires towards efficient solar cells," *Nano Today*, vol. 11, no. 6, pp. 704–737, Dec. 2016.

[21] Z. Y. Li, H. H. Tan, C. Jagadish, and L. Fu, "III-V semiconductor single nanowire solar cells: A review," *Adv. Mater. Technol.*, vol. 3, no. 9, Sep. 2018, Art. no. 1800005.

[22] G. Kang, J. Yoo, J. Ahn, and K. Kim, "Transparent dielectric nanostructures for efficient light management in optoelectronic applications," *Nano Today*, vol. 10, no. 1, pp. 22–47, Feb. 2015.

[23] E. Garnett and P. D. Yang, "Light trapping in silicon nanowire solar cells," *Nano Lett.*, vol. 10, no. 3, pp. 1082–1087, Mar. 2010.

[24] W. I. Nam, Y. J. Yoo, and Y. M. Song, "Geometrical shape design of nanophotonic surfaces for thin film solar cells," *Opt. Exp.*, vol. 24, no. 14, pp. A1033–A1044, Jul. 2016.

[25] A. H. Trojnar, C. E. Valdivia, R. R. Lapierre, K. Hinzer, and J. J. Krich, "Optimizations of GaAs nanowire solar cells," *IEEE J. Photovolt.*, vol. 6, no. 6, pp. 1494–1501, Nov. 2016.

[26] D. V. Prashant, D. P. Samajdar, and D. Sharma, "Optical simulation and geometrical optimization of P3HT/GaAs nanowire hybrid solar cells for maximal photocurrent generation via enhanced light absorption," *Sol. Energy*, vol. 194, pp. 848–855, Dec. 2019.

[27] Y. G. Ro et al., "Surface passivation and carrier collection in {110}, {100} and circular Si microwire solar cells," *Adv. Energy Mater.*, vol. 8, no. 33, Nov. 2018, Art. no. 1802154.

[28] X. Fang et al., "Hierarchically ordered silicon metastructures from improved self-assembly-based nanosphere lithography," *Amer. Chem. Soc. Appl. Mater. Interfaces*, vol. 12, no. 10, pp. 12345–12352, Mar. 2020.

[29] K. T. Fountaine, W. H. Cheng, C. R. Bukowsky, and H. A. Atwater, "Near-unity unselective absorption in sparse InP nanowire arrays," *Amer. Chem. Soc. Photon.*, vol. 3, no. 10, pp. 1826–1832, Oct. 2016.

[30] D. Van Dam et al., "High-efficiency nanowire solar cells with omnidirectionally enhanced absorption due to self-aligned indium-tin-oxide Mie scatterers," *Amer. Chem. Soc. Nano*, vol. 10, no. 12, pp. 11414–11419, Dec. 2016.

[31] B. C. P. Sturmberg et al., "Optimizing photovoltaic charge generation of nanowire arrays: A simple semi-analytic approach," *Amer. Chem. Soc. Photon.*, vol. 1, no. 8, pp. 683–689, Aug. 2014.

[32] G. Shalev, S. W. Schmitt, G. Brönstrup, and S. Christiansen, "Maximizing the ultimate absorption efficiency of vertically-aligned semiconductor nanowire arrays with wires of a low absorption cross-section," *Nano Energy*, vol. 12, pp. 801–809, Mar. 2015.

[33] L. Cao, "Optical resonances of semiconductor nanowires," Ph.D. dissertation, Stanford University, Stanford, CA, USA, 2010.

[34] K. M. Azizur-Rahman and R. R. Lapierre, "Wavelength-selective absorptance in GaAs, InP and InAs nanowire arrays," *Nanotechnology*, vol. 26, no. 29, Jul. 2015, Art. no. 295202.